Interpolation of Fire Radiative Power in West Kalimantan using Ordinary Kriging

Gita Fitriyana[1], Nurfitri Imro'ah[1*], Nur'ainul Miftahul Huda[2], Zuleha[2]
[1]Department of Statistics, Universitas Tanjungpura, Indonesia
[2]Department of Mathematics, Universitas Tanjungpura, Indonesia
nurainul@fmipa.untan.ac.id

ABSTRACT

Forest fires are recurring environmental disasters with severe ecological and economic impacts, particularly in regions like West Kalimantan. One of the key indicators used to measure fire intensity is Fire Radiative Power (FRP). Accurate spatial prediction of FRP is essential to support early warning systems and mitigation strategies. This study is a quantitative descriptive research that applies a geostatistical spatial analysis technique, namely Ordinary Kriging interpolation, to predict FRP values in West Kalimantan for July, August, and September 2024. The data were obtained from satellite imagery (VIIRS NOAA-20), including latitude, longitude, and FRP values. Prior to modeling, data were tested for normality and found to follow a normal distribution. The spherical semivariogram model yielded the best fit for July and August with RMSE values of 0.046 and 0.011, respectively, while the Gaussian model was optimal for September (RMSE = 0.007). The results show spatial variation in FRP distribution across different regencies each month, with the highest estimated FRP values recorded in Kapuas Hulu (July: 63.56), Melawi (August: 69.00), and Ketapang (September: 55.27). Most areas demonstrated low fire intensity, as shown by the dominance of green zones on the prediction maps. However, localized red-yellow zones indicate areas with high fire potential, which shifted monthly. This study contributes by demonstrating the application of Ordinary Kriging in forest fire intensity mapping and highlights the importance of choosing an appropriate semivariogram model to enhance predictive accuracy. The resulting FRP prediction maps can serve as a valuable tool for policy planning and targeted fire prevention efforts.

—————————— ◆ ——————————

A. INTRODUCTION

Fire Radiative Power (FRP) is a fundamental parameter for fire characterization because it represents the fire's heat emission rate (Filizzola et al., 2023). In addition, FRP is a key indicator used to assess wildfire intensity, as it provides more detailed quantitative information than conventional fire lines or burned area maps, which typically offer only binary data. Operational remote sensing techniques for estimating FRP have been developed and widely applied over the past two decades to evaluate combustion and emission rates (S. S. Kumar et al., 2020), highlighting its long-standing relevance in wildfire research. It also plays a crucial role in the real-time detection and monitoring of fires. Mapping spatial FRP values is vital in efforts to mitigate and control forest fires. Therefore, accurate FRP prediction is essential not only to support more effective firefighting actions but also to evaluate the environmental pollution impacts associated with wildfires (Dong et al., 2024).

Forest fires are one of the major environmental disasters with widespread impacts in Indonesia. This is driven by the increasing demand for land use for agriculture and residential development (Pratiwi et al., 2025). Land-use changes, particularly the conversion to oil palm plantations, are a primary cause of forest fires in peatland areas. Forest fires, also referred to as bushfires or vegetation fires, can also be triggered by climatic changes, which are intensified by high greenhouse gas emissions and global warming (Supriya & Gadekallu, 2023). In fact, human activities are responsible for over 90% of forest fires, while the remaining cases are mostly caused by natural events such as lightning strikes (Alkhatib et al., 2023). Wildfires occur globally and have significant impacts on ecosystems, the environment, human populations, and infrastructure (Thom & Seidl, 2016). The consequences of these fires can lead to thick smoke, causing ecosystem damage, public health issues, transportation disruptions, and a significant decline in air quality. Each year, substantial financial resources are allocated to fire management initiatives aimed at preventing or controlling forest fires (Borrelli et al., 2015), yet the scale and frequency of fire events remain a serious concern.

Forest fires have become a serious environmental issue in recent years, especially on the island of Kalimantan, which is part of Borneo and frequently faces this problem (Huda & Imro'ah, 2024). One of the regions often affected is West Kalimantan Province. Forest fires in West Kalimantan continue to seriously threaten the environment and human life (Huda et al., 2025). This scenario is influenced by a mix of natural elements, such as extended drought periods and the El Niño weather pattern, alongside anthropogenic actions like land clearing via burning. In particular, on peatlands, the risk of forest fires increases during dry climates and high temperatures (Pratiwi et al., 2025).

FRP is considered spatial data because each observation point of FRP is associated with important geographic attributes, namely latitude and longitude. Spatial analysis involves examining data with a focus on the location or distance between objects (Xu & Kennedy, 2015). Spatial data is analyzed to understand patterns and relationships between locations, distributions, or geographic trends. Spatial analysis is a quantitative study of spatial phenomena in geography and even earth science (Chen et al., 2020), aiming to uncover spatial patterns and dependencies in environmental and geospatial data. Spatial analysis is the process of processing, modeling, and interpreting data related to geographic or spatial locations on the Earth's surface (Franch-Pardo et al., 2020). The term spatial analysis describes methods to study the location, distribution, and relationship of spatial phenomena (Bäing, 2023).

The Ordinary Kriging method is one of the most widely used spatial analysis methods. This technique estimates the value at a specific point within a region where the variogram is known, utilizing data from surrounding locations (Meliyana R. & Ahmar, 2023). Kriging is the most effective linear, optimal, unbiased interpolation technique for estimating unknown values of spatial and temporal variables while minimizing mean interpolation error (Chung et al., 2019). Nonetheless, the proper implementation of Ordinary Kriging necessitates a precise assessment of the spatial structure through the construction of a semivariogram and subsequent model-fitting (Emmanuel et al., 2020). In this study, Ordinary Kriging is applied to predict FRP values in the West Kalimantan region to illustrate the spatial distribution of forest and land fire intensity based on FRP data.

Several previous researchers have conducted the prediction of FRP using spatial approaches. For example, studies using FRP data from MODIS satellites in countries such as Nepal, Bhutan, and Sri Lanka employed spatial statistical methods like the Spatial Lag Model, Spatial Error Model, and Kriging to map and predict the spatial distribution of FRP. The Kriging interpolation technique was used to estimate fire potential in areas not directly observed, providing a comprehensive overview of fire risk and impact (Devkota, 2021). Another study in Florida, USA, used Fire Radiative Energy Density (FRED) data, Ordinary Kriging, and Gaussian Conditional Simulation methods to interpolate FRED values in unmonitored areas. The resulting interpolation provided accurate estimations (Klauberg et al., 2018). Additionally, a study in Kubu Raya Regency, West Kalimantan, applied Kriging interpolation to analyze the spatial distribution of peatland fire hotspots, highlighting the spread of fire risk to surrounding areas based on historical satellite data (Huda et al., 2025).

This study aims to predict the spatial distribution of Fire Radiative Power (FRP) in West Kalimantan Province using the Ordinary Kriging method. The objective is to produce spatially continuous maps that identify fire intensity patterns across the region, thereby supporting better-informed decisions for fire management and environmental protection. The novelty of this study lies in its integration of FRP data from the VIIRS NOAA-20 sensor and semivariogram-based spatial interpolation to offer a refined prediction of fire potential in a high-risk region.

B. METHODS

This study employs a quantitative descriptive research approach that focuses on spatial analysis using geostatistical interpolation. The aim is to describe and model the spatial distribution of Fire Radiative Power (FRP) in West Kalimantan using the Ordinary Kriging method.

1. Kriging

Kriging is a group of geostatistics-based interpolation techniques that attempt to give an unbiased estimate of the value of a variable on a surface (Wu, 2017). Kriging weights are defined by two conditions: the value to be estimated and its estimator have the same average value, and the estimation error variance, or prediction variance, is the minimum feasible value (Freulon & Desassis, 2023). Points that are closer to the estimation location are given higher weights compared to those that are farther away. The estimation accuracy is highly influenced by the shape of the semivariogram model used to determine these weights. The Kriging model can be represented by the following equation (Pham et al., 2019):

$$\hat{Z}(u_0) = \sum_{i=1}^{n} w_i Z(u_0) \tag{1}$$

The estimated value at location u_0 is denoted as $\hat{Z}(u_0)$, which is a linear combination of the observed values $\hat{Z}(u_i)$ at locations u_i, each multiplied by a corresponding weight w_i. The number of observation points used in the estimation is represented by n. The weights w_i are determined based on the distance and spatial relationship between the points. Generally, several types of kriging methods are available: ordinary, simple, universal, Poisson probability, and more (Böhner & Bechtel, 2018). However, this study employs the Ordinary Kriging method.

The object of this study is Fire Radiative Power (FRP) data for West Kalimantan Province, obtained from the VIIRS (Visible Infrared Imaging Radiometer Suite) sensor onboard the NOAA-20 satellite. The data were accessed through the FIRMS NASA website and cover the period of July, August, and September 2024. Prior to analysis, the data were downloaded in SHP format, filtered to include only observations within the West Kalimantan region, and processed in GIS software to extract relevant spatial information. The FRP values along with their geographic coordinates were then prepared for use in the Kriging interpolation process.

2. Variogram and Semivariogram

A variogram is a function that describes the degree of difference or variation between pairs of data points separated by a certain distance. This function assesses the spatial relationship between data points based on their separation distance. The variogram is formulated as follows:

$$2\gamma(h) = \frac{1}{N(h)} \sum_{i=1}^{N(h)} [Z(u_i + h) - Z(u_i)]^2 \tag{2}$$

where $2\gamma(h)$ is the variogram at distance h, $Z(u)$ is the observed value at location u, $Z(u + h)$ is the observed value at location $(u + h)$, and $N(h)$ is the number of point pairs separated by distance h.

The semivariogram is defined as half the value of the variogram. In general, semivariograms are classified into two types: experimental semivariogram and theoretical semivariogram. The experimental semivariogram is a plot of semivariance values $\gamma(h)$ against distance h (Setiyoko et al., 2020). The experimental semivariogram is calculated based on observed or sample data using the following formula (Xia et al., 2020):

$$\gamma(h) = \frac{1}{N(h)} \sum_{i=1}^{N(h)} [Z(u_i + h) - Z(u_i)]^2 \tag{3}$$

where $\gamma(h)$ represents the semivariogram value at distance h.

The value of the experimental semivariogram will later be compared with the theoretical semivariogram to determine the best-fitting model to be used in the weighting process of the Kriging method. Theoretical semivariograms generally consist of three types of models, namely (Wong & Kwon, 2021):

   a. Exponential Model

     The exponential model describes a sharp increase in variance at short distances, which then gradually levels off as the distance increases. The exponential model is formulated as follows:

$$\gamma(h) = c(1 - exp(-h/a))$$

b. Spherical Model

The spherical model is a semivariogram model where spatial variability increases linearly with distance up to a certain range, after which it levels off at the sill. The spherical model is formulated as follows:

$$\gamma(h) = c\left[\frac{3}{2}\left(\frac{h}{a}\right) - \frac{1}{2}\left(\frac{h}{a}\right)^3\right], \text{if } h \le a$$
$$\gamma(h) = c, \text{if } h > a$$

c. Gaussian Model

The Gaussian model shows a very gradual increase in variance at short distances, followed by a sharper rise as the distance approaches the range. The Gaussian semivariogram model is formulated as follows:

$$\gamma(h) = c\left[1 - exp\left(\left(\frac{h}{a}\right)\right)\right]$$

where h represents the distance between sample locations, c is the sill (the value where the semivariogram levels off), and a is the range (the distance at which spatial correlation effectively becomes zero). The graphs of the three theoretical semivariogram models are presented in Figure 1 (Hilal et al., 2024):
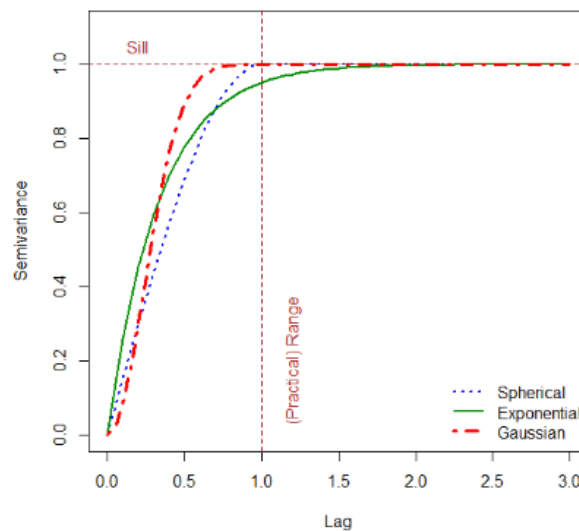

Figure 1. Theoretical semivariogram model

3. Ordinary Kriging

Ordinary Kriging is a method that assumes the population mean is unknown but remains constant throughout the study area (Sukkuea & Heednacram, 2022). It operates under the assumption that the mean is not explicitly known but does not vary spatially. In Ordinary Kriging, spatial prediction is based on several underlying assumptions (P. Kumar et al., 2023). The Ordinary Kriging equation is given as follows:

$$\hat{Z}(u_0) = \sum_{i=1}^{n} w_i Z(u_0) \tag{4}$$

with $\sum_{i=1}^{n} w_i = 1$, where $\hat{Z}(u_i)$ denotes the estimated value at location u_i, n represents the number of samples used for estimation, and w_i is the weight assigned to each variable. One of the main objectives of the Kriging method is to produce an estimate that meets the three criteria of a Best Linear Unbiased Estimator (BLUE) (Li et al., 2021).

 a. Linear, the estimate $\hat{Z}(u_0)$ is considered linear because it is formed as a linear combination of the observed values $\hat{Z}(u_i)$.

 b. Unbiased, the Ordinary Kriging method produces unbiased estimates because the sum of the weights is equal to one, i.e., $\sum_{i=1}^{n} w_i = 1$, ensuring that the expected value of the estimation equals the true mean.

 c. Best, the Ordinary Kriging method produces estimates with the smallest possible error variance, making it the most precise linear unbiased estimator. The variance of the estimation error is expressed as:

$$Var(e(u_0)) = \sigma^2 - \left[\sum_{i=1}^{n} w_i Cov\left(Z(u_i), Z(u_0)\right) - \lambda \right]$$
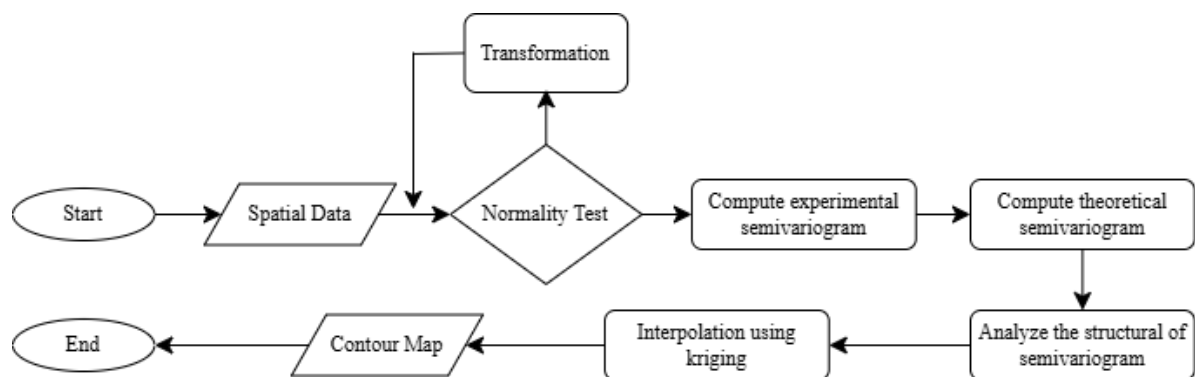

Figure 2. Ordinary Kriging analysis flowchart

C. RESULT AND DISCUSSION

The data used in this study are Fire Radiative Power (FRP) values obtained from the NOAA-20 VIIRS satellite. Data were obtained through the NASA FIRMS website covering the West Kalimantan Province in July, August, and September 2024 (NASA, 2024). The data collected includes three main variables, namely longitude in decimal degrees as the X variable (abscissa), latitude in decimal degrees as the Y variable (ordinate), and FRP values, which are used in the analysis to map and predict the distribution pattern of fire intensity levels in the West Kalimantan region using the Ordinary Kriging method. The distribution of FRP data in July, August, and September 2024 can be seen in Figure 3.
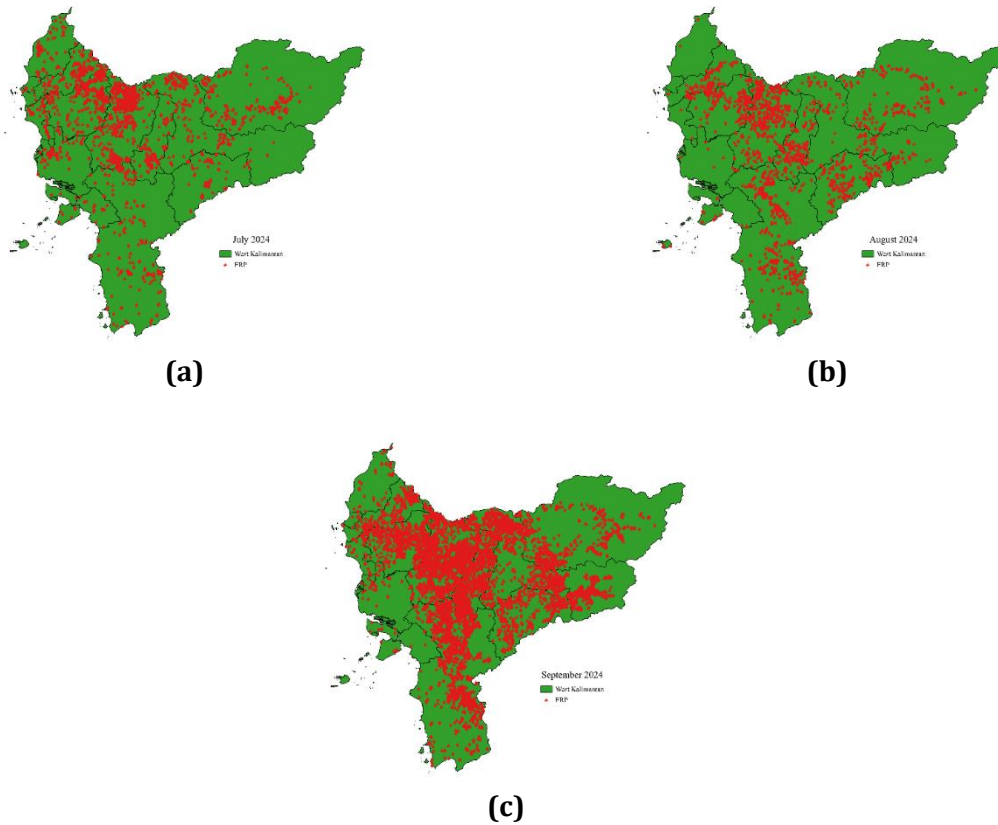
(a)

(b)

(c)

Figure 3. Map of FRP distribution in West Kalimantan in 2024 in the months of (a) July (b) August (c) September

The data shows that July, August, and September are the months with the highest levels of fire intensity in West Kalimantan in 2024. This can be seen in Figure 3, which shows that September has the highest distribution of fire intensity levels throughout 2024. July is in second place with 3,347 FRP points and has the lowest FRP value of 0.20 in the Mempawah Regency and the highest FRP value of 321.64 in the Landak Regency. The third place is in August, with 2,317 FRP points. However, August has the highest FRP value among other months, namely 341.73 in Kapuas Hulu Regency and the lowest value of 0.39 in Ketapang Regency. August also has very varied FRP values , with a distribution level 310.03 and an average of 12.64. Although the number of hotspots is smaller, this month shows a more severe fire intensity due to extreme fire incidents in specific locations. Meanwhile, in September, there was a widespread spread of fires, but with a low and stable level of fire intensity. This is indicated by the low variance value compared to other months, which is 237.14, and an average value of 12.41. The minimum FRP value in September occurred in the Sintang district of 0.26, and the highest FRP value occurred in the Landak district of 254.78. A summary of these values is presented in Table 1.

Table 1. Descriptive Statistics

Values	July	August	September
Mean	11.33	12.64	12.41
Varians	252.28	310.03	237.14
Minimum	0.20	0.39	0.26
Maximum	321.64	341.73	254.78
Number of Points	3,347	2,317	9,724

1. **Normality**

The normality test was conducted to determine whether the FRP data used in this study was normally distributed. The non-normality may cause potential issues when fitting a kriging model, particularly during the covariance function fitting stage (Guo & Li, 2024). The normality test was conducted using the Kolmogorov-Smirnov test with the following hypothesis.

Hypothesis:

$H_0: \pi = 0 =$ Data are normally distributed

$H_1: \pi \neq 0 =$ Data are not normally distributed

Rejection region:

Reject H_0 if the p-value $< \alpha$ (0.05)

Table 2. Normality test

P-Value Kolmogorov-Smirnov Test		
July	**August**	**September**
2.2×10^{-16}	2.2×10^{-16}	2.2×10^{-16}

Based on Table 2, it can be seen that the p-value $< \alpha$ (0.05), which means that H_0 is rejected. This indicates that the July, August, and September data are not normally distributed. Therefore, a logarithmic transformation was applied to all three datasets to produce unbiased predictions.

2. **Experimental Semivariogram**

After the data were transformed, the next step was calculating the experimental semivariogram values based on the coordinates and FRP values for July, August, and September. The results of the experimental semivariogram calculations are presented in Table 3.

Table 3. Experimental semivariogram

Class	July			August			September		
	Range (h)	**$N(h)$**	**$\gamma(h)$**	**Range (h)**	**$N(h)$**	**$\gamma(h)$**	**Range (h)**	**$N(h)$**	**$\gamma(h)$**
1	0.076	160,923	0.784	0.091	486,96	0.695	0.097	712,427	0.730
2	0.224	196,704	0.778	0.231	934,48	0.701	0.238	1,610,319	0.745
3	0.365	253,423	0.810	0.380	120,725	0.726	0.389	2,279,614	0.748
4	0.515	272,220	0.823	0.530	138,302	0.723	0.542	2,710,580	0.758
5	0.659	312,903	0.818	0.679	142,350	0.691	0.695	3,042,599	0.766
6	0.805	349,978	0.861	0.832	156,052	0.688	0.849	3,209,641	0.772
7	0.950	405,590	0.905	0.982	161,139	0.686	1.003	3,345,087	0.772
8	1.095	417,460	0.956	1.132	168,986	0.701	1.157	3,357,203	0.778
9	1.241	414,801	0.891	1.283	158,689	0.709	1.312	3,351,592	0.769
10	1.388	399,023	0.913	1.434	153,826	0.712	1.466	3,367,047	0.760
11	1.533	413,884	0.872	1.587	160,583	0.706	1.619	3,155,980	0.754
12	1.675	326,919	0.925	1.737	165,901	0.708	1.774	2,960,982	0.754
13	1.824	206,372	0.923	1.886	159,118	0.706	1.928	2,625,131	0.759
14	1.971	170,861	0.936	2.036	134,843	0.715	2.081	2,302,133	0.752
15	2.121	175,190	0.964	2.188	117,962	0.711	2.236	1,914,156	0.749

The next step is to calculate the semivariogram parameters, namely the sill, nugget, and range, in order to determine the appropriate theoretical model. The results of the semivariogram parameter calculations are presented in Table 4.

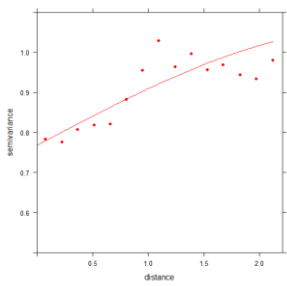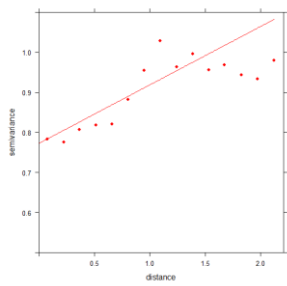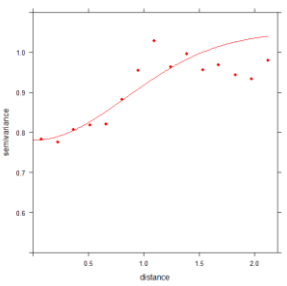**Table 4.** Semivariogram parameter values

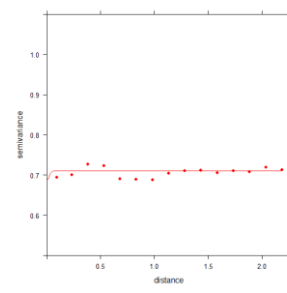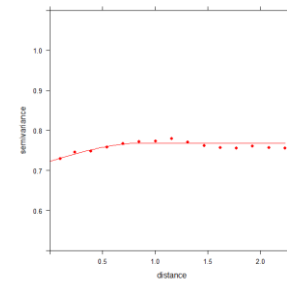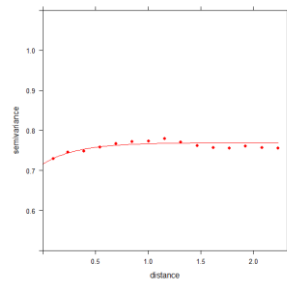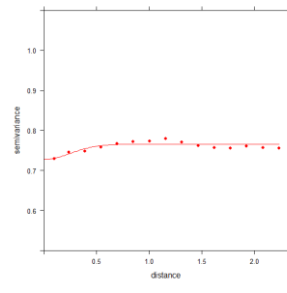| Model	Parameter	July	August	September
Spherical	Sill	0.768	0.684	0.723
	Nugget	1.064	0.709	0.769
	Range	3.021	0.173	0.877
Exponential	Sill	0.773	0.686	0.716
	Nugget	55.874	0.686	0.769
	Range	375.726	0.729	0.331
Gaussian	Sill	0.780	0.688	0.727
	Nugget	1.052	0.710	0.766
	Range	1.185	0.029	0.352
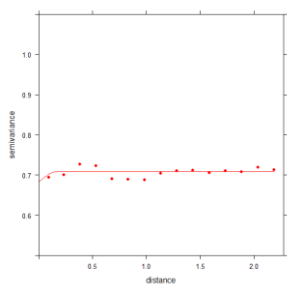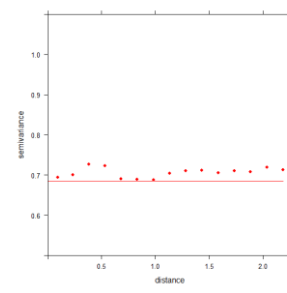
After determining the parameter values for each model, the next step is to create semivariogram plots to identify which model best fits the data pattern. In addition, the best semivariogram model is selected based on the Root Mean Square Error (RMSE) value. The Kriging method is considered to have good estimation accuracy if it yields the smallest RMSE value (Oliver & Webster, 2015). The RMSE can be calculated using the following formula (Id et al., 2022):

$$RMSE = \sqrt{\frac{1}{n}\sum_{i=1}^{n}(y_i - \hat{y}_i)^2}$$

where n is the number of data points, y_i is the actual value, and $\hat{y}_i$ is the predicted value. The RMSE values and semivariogram plots are presented in Table 5.

Table 5. Model selection based on RMSE

Model	Spherical	Exponential	Gaussian
		July	
RMSE	0.046	0.060	0.049
Plot			
		August	
RMSE	0.011	0.024	0.012

Model	Spherical	Exponential	Gaussian
Plot			
September			
RMSE	0.008	0.009	0.007
Plot			

Based on Table 5, it can be observed that the best semivariogram model used in July and August is the Spherical model, with RMSE values of 0.046 and 0.011, respectively. Meanwhile, in September, the Gaussian model was identified as the best fit, with the lowest RMSE value of 0.007. The RMSE values highlighted in bold indicate the lowest prediction error among the models compared. Therefore, by selecting the optimal semivariogram model, more precise estimation results can be obtained, as the chosen model accurately represents the spatial variation in the data. This, in turn, supports better decision-making and interpretation in spatial analysis.

3. Estimation of Fire Radiative Power (FRP) at Unobserved Locations

Based on the results of Kriging interpolation, the highest estimated FRP value in July was found in Kapuas Hulu Regency at 63.56, while the lowest was in Melawi Regency at 0.57. In August, Melawi Regency recorded the highest estimated FRP value at 69.61, and Ketapang Regency had the lowest at 0.82. In September, the highest estimated FRP value was in Ketapang Regency at 91.04, and the lowest was in Bengkayang Regency at 1.02. The spatial distribution of estimated FRP values for July, August, and September is shown in Figure 4 below.
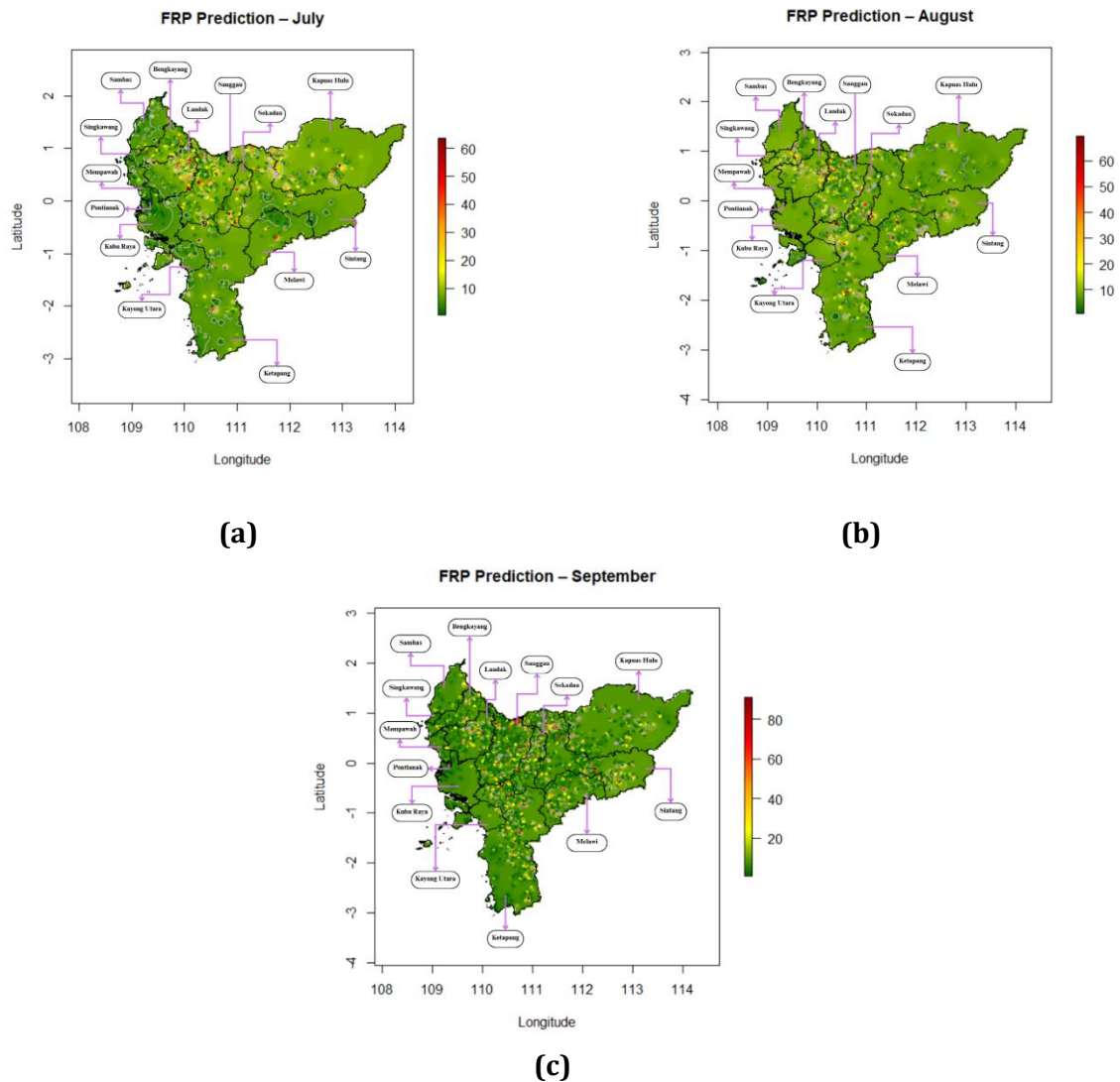
Figure 4. Spatial distribution maps of estimated FRP in West Kalimantan in 2024 for the months of (a) July, (b) August, and (c) September

Figure 4 further illustrates how the intensity and location of fire activity fluctuate over time. While most regions consistently exhibit low FRP values as shown by the dominance of green tones on the maps there are pockets of persistently high FRP areas, particularly in central and southern West Kalimantan. These spatial-temporal variations suggest that fire activity is not static but dynamically responds to changes in short-term climatic conditions, such as rainfall variability, as well as anthropogenic influences like peatland disturbance and agricultural practices. For instance, the lower FRP values in August compared to July and September may be attributed to temporary rainfall events, which suppressed fire intensity. However, the reemergence of high FRP in September especially in Ketapang indicates a return to drier conditions or sustained fire sources. This pattern highlights the importance of monitoring monthly changes, as areas that appear inactive in one month may quickly become hotspots in the next. These results support previous findings in Kubu Raya Regency, which also demonstrated significant spatial clustering and temporal shifts in fire intensity based on Kriging analysis (Huda et al., 2025). The consistency between this study and earlier research

reinforces the understanding that fire risk in West Kalimantan is highly localized and shaped by both environmental variability and ongoing land-use dynamics.

D. CONCLUSION AND SUGGESTIONS

The study revealed that the spatial distribution and intensity of fire activity in West Kalimantan during July, August, and September 2024 exhibited clear spatial variability across regions and time. Although most areas showed low FRP, some regions consistently exhibited higher intensity, indicating localized fire risk zones. The applied Ordinary Kriging method, supported by low RMSE values (ranging from 0.007 to 0.046), confirms the reliability of the spatial predictions made in this study. These findings offer valuable insights for improving fire mitigation strategies, enabling authorities to prioritize high-risk areas for surveillance and resource allocation. Furthermore, the spatial modelling approach used in this study can support the development of predictive tools and inform future research on fire dynamics in relation to climate patterns and land use.

REFERENCES

Alkhatib, R., Sahwan, W., Alkhatieb, A., & Schütt, B. (2023). A Brief Review of Machine Learning Algorithms in Forest Fires Science. In *Applied Sciences* (Vol. 13, Issue 14, pp. 1–15). https://doi.org/10.3390/app13148275

Bäing, A. S. (2023). *Spatial Analysis BT - Encyclopedia of Quality of Life and Well-Being Research* (F. Maggino (ed.); pp. 6774–6776). Springer International Publishing. https://doi.org/10.1007/978-3-031-17299-1_2818

Böhner, J., & Bechtel, B. (2018). *2.10 - GIS in Climatology and Meteorology* (B. B. T.-C. G. I. S. Huang (ed.); pp. 196–235). Elsevier. https://doi.org/10.1016/B978-0-12-409548-9.09633-0

Borrelli, P., Armenteras, D., Panagos, P., Modugno, S., & Schütt, B. (2015). The Implications of Fire Management in the Andean Paramo: A Preliminary Assessment Using Satellite Remote Sensing. In *Remote Sensing* (Vol. 7, Issue 9, pp. 11061–11082). https://doi.org/10.3390/rs70911061

Chen, Q., Liu, G., Ma, X., & Que, X. (2020). *Spatial Analysis BT - Encyclopedia of Mathematical Geosciences* (B. S. Daya Sagar, Q. Cheng, J. McKinley, & F. Agterberg (eds.); pp. 1–3). Springer International Publishing. https://doi.org/10.1007/978-3-030-26050-7_300-1

Chung, S. Y., Venkatramanan, S., Elzain, H. E., Selvam, S., & Prasanna, M. V. (2019). Supplement of Missing Data in Groundwater-Level Variations of Peak Type Using Geostatistical Methods (Chapter 4, pp. 33–41). In S. Venkatramanan, M. V. Prasanna, & S. Y. Chung (Eds.), GIS and geostatistical techniques for groundwater science. Elsevier. https://doi.org/10.1016/B978-0-12-815413-7.00004-3

Devkota, J. U. (2021). Statistical Analysis of Active Fire Remote Sensing Data: Examples From South Asia. *Environmental Monitoring and Assessment*, *193*(9), 608. https://doi.org/10.1007/s10661-021-09354-x

Dong, Z., Zheng, C., Zhao, F., Wang, G., Tian, Y., & Li, H. (2024). A Deep Learning Framework: Predicting Fire Radiative Power From the Combination of Polar-Orbiting and Geostationary Satellite Data During Wildfire Spread. *IEEE Journal of Selected Topics in Applied Earth Observations and Remote Sensing*, *17*, 10827–10841. https://doi.org/10.1109/JSTARS.2024.3403146

Emmanuel, O. R., Y., S. A., & B., O. M. (2020). Assessment of Ordinary Kriging and Inverse Distance Weighting Methods for Modeling Chromium and Cadmium Soil Pollution in E-Waste Sites in Douala, Cameroon. *Journal of Health and Pollution*, *10*(26), 200605. https://doi.org/10.5696/2156-9614-10.26.200605

Filizzola, C., Falconieri, A., Lacava, T., Marchese, F., Masiello, G., Mazzeo, G., Pergola, N., Pietrapertosa, C., Serio, C., & Tramutoli, V. (2023). Fire Characterization by Using an Original RST-Based Approach for Fire Radiative Power (FRP) Computation. *Fire*, *6*(2), 1–18. https://doi.org/10.3390/fire6020048

Franch-Pardo, I., Napoletano, B. M., Rosete-Verges, F., & Billa, L. (2020). Spatial analysis and GIS in the study of COVID-19. A review. *Science of The Total Environment*, *739*, 140033. https://doi.org/https://doi.org/10.1016/j.scitotenv.2020.140033

Freulon, X., & Desassis, N. (2023). *Kriging BT - Encyclopedia of Mathematical Geosciences* (B. S. Daya Sagar, Q. Cheng, J. McKinley, & F. Agterberg (eds.); pp. 705–713). Springer International Publishing. https://doi.org/10.1007/978-3-030-85040-1_18

Guo, Y., & Li, J. S.-H. (2024). Kriging Methods for Modeling Spatial Basis Risk in Weather Index Insurances: A Technical Note. *International Journal of Theoretical and Applied Finance*, *27*(01), 2350034. https://doi.org/10.1142/S0219024923500346

Hilal, A., Bangroo, S. A., Kirmani, N. A., Wani, J. A., Biswas, A., Bhat, M. I., Farooq, K., Bashir, O., & Shah, T. I. (2024). Chapter 19 - Geostatistical Modeling a Tool for Predictive Soil Mapping. In S. Lamine, P. K. Srivastava, A. Kayad, F. Muñoz-Arriola, & P. C. B. T.-R. S. in P. A. Pandey (Eds.), *Earth Observation* (pp. 389–418). Academic Press. https://doi.org/10.1016/B978-0-323-91068-2.00011-4

Huda, N. M., & Imro'ah, N. (2024). Modeling the Dynamics of Forest Fires : A Vector Autoregressive Approach Across Three Fire Classifications. *Jurnal Teori Dan Aplikasi Matematika*, *8*(4), 1157–1168. https://doi.org/10.31764/jtam.v8i4.24792

Huda, N. M., Imro'ah, N., Ayyash, M. Y., & Pratiwi, H. (2025). Forest Fires in Peatlands Analyzed from Various Perspectives : Spatial , Temporal , and Spatial-Temporal. *Jurnal Teori Dan Aplikasi Matematika*, *9*(2), 482–496. https://doi.org/10.31764/jtam.v9i2.28884

Id, Y. L., Baorong, Z., Xiaohong, X., & Zijun, L. (2022). Application of a Semivariogram Based on a Deep Neural Network to Ordinary Kriging Interpolation of Elevation Data. *PLOS ONE*, *17*(4), 1–12. https://doi.org/10.1371/journal.pone.0266942

Klauberg, C., Hudak, A., Bright, B., Boschetti, L., Dickinson, M., Kremens, R., & Silva, C. (2018). Use of Ordinary Kriging and Gaussian Conditional Simulation to Interpolate Airborne Fire Radiative Energy Density Estimates. *Supplementary Material: International Journal of Wildland Fire*, *27*(4), 228–240. 10.1071/WF17113

Kumar, P., Rao, B., Burman, A., Kumar, S., & Samui, P. (2023). Spatial Variation of Permeability and Consolidation Behaviors of Soil Using Ordinary Kriging Method. *Groundwater for Sustainable Development*, *20*, 100856. https://doi.org/https://doi.org/10.1016/j.gsd.2022.100856

Kumar, S. S., Hult, J., Picotte, J., & Peterson, B. (2020). Potential Underestimation of Satellite Fire Radiative Power Retrievals over Gas Flares and Wildland Fires. In *Remote Sensing* (Vol. 12, Issue 2, pp. 1–9). https://doi.org/10.3390/rs12020238

Li, M., Shen, S., Barzegar, V., Sadoughi, M., Hu, C., & Laflamme, S. (2021). Kriging-Based Reliability Analysis Considering Predictive Uncertainty Reduction. *Structural and Multidisciplinary Optimization*, *63*(6), 2721–2737. https://doi.org/10.1007/s00158-020-02831-w

Meliyana R., S. M., & Ahmar, A. S. (2023). Analysis of the Distribution of Diarrhea Patients in Bogor Regency Month Using the Ordinary Kriging Method. *ARRUS Journal of Social Sciences and Humanities*, *3*(2), 156–162. https://doi.org/10.35877/soshum1727

NASA. (2024). *FIRMS Active Fire Data Download*. https://firms.modaps.eosdis.nasa.gov/download/create.php

Oliver, M. D., & Webster, R. (2015). *Basic Steps in Geostatistics: The Variogram and Kriging*. SpringerBriefs in Agriculture. https://link.springer.com/book/10.1007/978-3-319-15865-5

Pham, T. G., Kappas, M., Huynh, C. Van, & Nguyen, L. H. K. (2019). Application of Ordinary Kriging and Regression Kriging Method for Soil Properties Mapping in Hilly Region of Central Vietnam. *ISPRS International Journal of Geo-Information*, *8*(3), 147. https://doi.org/10.3390/ijgi8030147%0A

Pratiwi, H., Imro'ah, N., & Huda, N. M. (2025). Forest Fire Analysis From Perspective of Spatial-Temporal Using GSTAR Model. *Barekeng: Journal of Mathematics and Its Applications*, *19*(2), 1379–1392.

Pratiwi, H., Imro'ah, N., Huda, N. M., & Ayyash, M. Y. (2025). Comparison of Weight Matrix in Hotspot Modeling in West Kalimantan Using The GSTAR Method. *Jurnal Matematika UNAND*, *14*(1), 31–45. https://doi.org/10.25077/jmua.14.1.31-45.2025

Setiyoko, A., Basaruddin, T., & Arymurthy, A. M. (2020). Minimax Approach for Semivariogram Fitting in Ordinary Kriging. *IEEE Access*, *8*, 82054–82065. https://doi.org/10.1109/ACCESS.2020.2991428

Sukkuea, A., & Heednacram, A. (2022). Prediction on Spatial Elevation Using Improved Kriging Algorithms: An Application in Environmental Management. *Expert Systems with Applications*, *207*, 117971. https://doi.org/10.1016/j.eswa.2022.117971

Supriya, Y., & Gadekallu, T. R. (2023). Particle Swarm-Based Federated Learning Approach for Early Detection of Forest Fires. In *Sustainability* (Vol. 15, Issue 2, pp. 1–19). https://doi.org/10.3390/su15020964

Thom, D., & Seidl, R. (2016). Natural Disturbance Impacts on Ecosystem Services and Biodiversity in Temperate and Boreal Forests. *Biological Reviews*, *91*(3), 760–781. https://doi.org/10.1111/brv.12193

Wong, Andy H, & Kwon, Tae J. (2021). Development and Evaluation of Geostatistical Methods for Estimating Weather Related Collisions: A Large-Scale Case Study. *Transportation Research Record*, *2675*(11), 828–840. https://doi.org/10.1177/03611981211020008

Wu, C. (2017). Interpolation: Kriging. In *International Encyclopedia of Geography*. https://doi.org/10.1002/9781118786352.wbieg0996

Xia, H., Zha, S., Huang, J., & Liu, J. (2020). Radio Environment Map Construction by Adaptive Ordinary Kriging Algorithm Based on Affinity Propagation Clustering. *International Journal of Distributed Sensor Networks*, *16*(5), 1550147720922484. https://doi.org/10.1177/1550147720922484

Xu, Y., & Kennedy, E. (2015). An Introduction to Spatial Analysis in Social Science Research. *The Quantitative Methods for Psychology*, *11*(1), 22–31. https://doi.org/10.20982/tqmp.11.1.p022